

The nucleon to Delta electromagnetic transition form factors in lattice QCD

C. Alexandrou and G. Koutsou

*Department of Physics, University of Cyprus, CY-1678, Cyprus**

H. Neff

Center for Computational Science, University College London, 20 Gordon Str., London WC1, UK

J.W. Negele

Center for Theoretical Physics, Massachusetts Institute of Technology, Cambridge, MA 02139, USA

W. Schroers

*Department of Physics, Center for Theoretical Sciences,
National Taiwan University, Taipei 10617, Taiwan†*

A. Tsapalis

University of Athens, Institute of Accelerating Systems and Applications, Athens, Greece

(Dated: October 24, 2018)

The electromagnetic nucleon to Δ transition form factors are evaluated using two degenerate flavors of dynamical Wilson fermions and using dynamical sea staggered fermions with domain wall valence quarks. The two subdominant quadrupole form factors are evaluated for the first time in full QCD to sufficient accuracy to exclude a zero value, which is taken as a signal for deformation in the nucleon- Δ system. For the Coulomb quadrupole form factor the unquenched results show deviations from the quenched results at low q^2 bringing dynamical lattice results closer to experiment, thereby confirming the importance of pion cloud contributions on this quantity.

PACS numbers: 11.15.Ha, 12.38.Gc, 12.38.Aw, 12.38.-t, 14.70.Dj

Keywords: Lattice QCD, Hadron deformation, Form Factors

I. INTRODUCTION

Despite several decades of scrutiny, the intrinsic shape of the nucleon, a fundamental building block of our world, is still not fully resolved [1, 2]. Although the nucleon is experimentally easily accessible in exclusive and inclusive scattering its spectroscopic quadrupole moment is zero since it has spin $J = 1/2$. However, this does not mean that the nucleon is spherically symmetric, since it can have an intrinsic deformation. Deformation is a common phenomenon in nuclear and atomic physics. Quantum mechanically, a multiphoton coincidence experiment could determine that a $J = 0$ ground state of a diatomic molecule or nucleus has a deformed shape. However, usually in electromagnetic probes of microscopic systems, we are constrained to make measurements associated with one-photon exchange, corresponding to a matrix element of a one-body operator. In the case of a diatomic molecule, the one-body charge density of the $J = 0$ state is spherically symmetric, and cannot reveal the deformation that is present in the system. For $J > 1/2$, however, when a nuclear or atomic system is well approximated by a deformed intrinsic state, it is still possible to observe its deformation using a one-body electromagnetic operator. In this case, the quadrupole moment is non-zero in the laboratory frame if the state is deformed. For collective rotation of the deformed intrinsic state [3], the relation between the spectroscopic quadrupole moment, Q , measured in the laboratory frame and the intrinsic quadrupole moment, Q_0 , in the body-fixed intrinsic frame is given by

$$Q = \frac{3K^2 - J(J+1)}{(J+1)(2J+3)} Q_0 \quad , \quad (1)$$

where J is the total angular momentum of the system in the laboratory frame, K is the projection of J onto the z-axis of the body-fixed intrinsic frame, and we have considered the sub-state with azimuthal quantum number $M = J$. In the previous example of the $J = 0$ diatomic molecule, although $Q_0 \neq 0$, Eq. (1) yields $Q = 0$ so that the deformation

*Electronic address: alexand@ucy.ac.cy

†Electronic address: Wolfram.Schroers@Field-theory.org

is unobservable. Similarly, in the case of a nucleon with $J = 1/2$, Q is zero although Q_0 may not be [4, 5]. Since the Δ has $J = 3/2$ a non-zero quadrupole moment Q can be measured [6]. The electric and Coulomb transition amplitudes E2 and C2 between the $J = 1/2$ nucleon and its $J = 3/2$ resonance have the same property of revealing the presence of deformation in the nucleon, the Δ , or both. Therefore, as in experiment, in this work we detect deformation by measuring E2 and C2.

In recent years, we have seen tremendous progress in experimental measurements of the subdominant quadrupole amplitudes [7, 8, 9, 10, 11, 12, 13, 14], yielding very accurate results particularly at low q^2 . For a recent review of the experimental situation see Ref. [15]. These accurate measurements have motivated several recent theoretical studies both in lattice QCD [16, 17, 18] and in chiral effective theories [19, 20]. On the lattice, hadron deformation can also be studied by investigating directly the charge distribution using density-density correlators [4, 21, 22], and it was shown that the rho meson is deformed [23]. The Δ shows deviations from a spherical shape albeit with large statistical errors. The issue of deformation of the Δ using density-density correlators is under study with improved lattice techniques [24, 25]. For concise reviews see [5, 26].

The focus of this work is a calculation of the nucleon - Δ electromagnetic transition form factors within QCD. We use two different types of simulations: The first uses two degenerate flavors of dynamical Wilson fermions and the second a hybrid action. The hybrid action uses dynamical staggered sea quarks, with two degenerate light quarks and one fixed to the mass of the strange quark. These dynamical quark configurations are produced by the MILC collaboration [27] and represent a state-of-the-art simulation of the QCD vacuum with the three lightest flavors of quarks taken into account. For the light valence quarks we use two degenerate domain wall fermions. This approach has been used successfully to evaluate nucleon structure functions [28, 29, 30, 31, 32, 33, 34] and the N to Δ axial-vector form factors [35, 36, 37, 38]. In this work, we compare results calculated using the hybrid action to the results obtained using two degenerate flavors of dynamical Wilson fermions. Given the different lattice artifacts involved in the two approaches, agreement between them provides a consistency check of our lattice methodology. Comparison between the dynamical results and our quenched results [16, 39] probes pion cloud contributions.

The first lattice study of the N to Δ electromagnetic transition form factors [40] was carried out in the quenched approximation with limited statistics. Although the mean value was negative, the statistical errors on the suppressed quadrupole amplitudes were large and a zero value could not be excluded. Nonetheless, this pioneering work set up the methodology for a more elaborate study that would soon become feasible once sufficient computing resources became available. Using the approach of Ref. [40] we evaluated the transition form factors using quenched and dynamical Wilson quarks going to smaller quark masses than those of Ref. [40] but only at the lowest q^2 -value allowed on our lattices [41]. However, although we increased statistics, the quadrupole form factors still had large errors. Constructing optimized sources that led to a large sample of statistically independent measurements for a given q^2 -value and carrying out sequential inversions through the source instead of through the current, we were finally able to obtain both quadrupole form factors to sufficient accuracy for a range of q^2 -values. This calculation, carried out in the quenched approximation, confirmed a non-zero value with the correct sign for both the quadrupole amplitudes [16]. Using this new methodology we extend in this work the calculation to the unquenched case. Initial unquenched results have been reported in Refs. [17, 18, 42].

Lattice calculations at the physical quark mass are currently prohibitively expensive. Recently, progress in both hardware performance and algorithms [43] has extended the range of accessible quark masses to lower masses, bringing lattice calculations into the region where they can be extrapolated using chiral perturbation theory. In this work, we use pions with masses as low as about 350 MeV. In a previous work [16], we found a discrepancy for the CMR ratio between the quenched lattice results and experiment at low values of q^2 . On the other hand, for larger q^2 -values, the quenched results and experiment were in quantitative agreement. Our current results for CMR show deviations between unquenched and quenched results at the lowest momentum transfer. In fact, the previously observed discrepancy is reduced by our new unquenched results. This could indicate that pion cloud effects are quite important at low q^2 and at light pion masses, as also discussed in the framework of chiral perturbation theory [44]. With pion masses in the range of 300 MeV as planned in the future one hopes to make progress in reliable chiral extrapolations to the physical regime. Such progress has been demonstrated recently in the extrapolation of the nucleon axial coupling within chiral effective theory [31, 45].

This paper is organized as follows: Section II gives the decomposition of the N to Δ matrix element on the hadronic level, Section III and Section IV detail the lattice analysis and outline our strategy for extracting observables. Section V contains our results for the transition form factors. Finally, Section VI contains our conclusions and an outlook for further studies we intend to perform in the field.

II. N TO DELTA MATRIX ELEMENT

The electromagnetic transition matrix element can be expressed in terms of the three Sachs form factors [46],

$$\langle \Delta(\mathbf{p}', s') | j_\mu | N(\mathbf{p}, s) \rangle = i \left(\frac{2}{3} \right)^{1/2} \left(\frac{m_\Delta m_N}{E_\Delta(\mathbf{p}') E_N(\mathbf{p})} \right)^{1/2} \bar{u}_\sigma(\mathbf{p}', s') \mathcal{O}_{\sigma\mu} \mathbf{u}(\mathbf{p}, s), \quad (2)$$

with the Lorentz-structure

$$\mathcal{O}_{\sigma\mu} = \mathcal{G}_{M1}(q^2) K_{\sigma\mu}^{M1} + \mathcal{G}_{E2}(q^2) K_{\sigma\mu}^{E2} + \mathcal{G}_{C2}(q^2) K_{\sigma\mu}^{C2}. \quad (3)$$

The kinematic prefactors in Euclidean space are given by

$$\begin{aligned} K_{\sigma\mu}^{M1} &= -\frac{3}{(m_\Delta + m_N)^2 + Q^2} \frac{m_\Delta + m_N}{2m_N} i \varepsilon_{\sigma\mu\alpha\beta} p^\alpha p'^\beta, \\ K_{\sigma\mu}^{E2} &= -K_{\sigma\mu}^{M1} + 6\Omega^{-1}(Q^2) \frac{m_\Delta + m_N}{2m_N} 2i \gamma_5 \varepsilon_{\sigma\lambda\alpha\beta} p^\alpha p'^\beta \varepsilon_\mu^{\lambda\gamma\delta} p_\gamma p'_\delta, \\ K_{\sigma\mu}^{C2} &= -6\Omega^{-1}(q^2) \frac{m_\Delta + m_N}{2m_N} i \gamma_5 q_\sigma (q^2(p + p')_\mu - q \cdot (p + p') q_\mu), \end{aligned} \quad (4)$$

where $p(s)$ and $p'(s')$ denote initial and final momenta (spins), $q^2 \equiv (p' - p)^2$, and $u_\sigma(p', s')$ is a spin-vector in the Rarita-Schwinger formalism. We define $\Omega(Q^2) = [(m_\Delta + m_N)^2 + Q^2] [(m_\Delta - m_N)^2 + Q^2]$ and $\mathbf{Q} = \mathbf{q}$, $Q^4 = iq^0$ is the lattice momentum transfer giving $Q^2 = -q^2$. The Rarita-Schwinger spin sum for the Δ in Euclidean space is given by

$$\sum_s u_\sigma(p, s) \bar{u}_\tau(p, s) = \frac{-i\gamma \cdot p + m_\Delta}{2m_\Delta} \left[\delta_{\sigma\tau} + \frac{2p_\sigma p_\tau}{3m_\Delta^2} - i \frac{p_\sigma \gamma_\tau - p_\tau \gamma_\sigma}{3m_\Delta} - \frac{1}{3} \gamma_\sigma \gamma_\tau \right], \quad (5)$$

and the Dirac spin sum

$$\sum_s u(p, s) \bar{u}(p, s) = \frac{-i\gamma \cdot p + m_N}{2m_N}. \quad (6)$$

The magnetic dipole form factor, \mathcal{G}_{M1} , is the dominant form factor. The electric and Coulomb quadrupole form factors, \mathcal{G}_{E2} , and \mathcal{G}_{C2} are subdominant. They are scalar functions depending on the momentum transfer squared. On the lattice we can only access space-like q^2 and therefore $Q^2 > 0$. The reason for using the Sachs parametrization in a lattice computation, as pointed out in Ref. [40], is that the Sachs form factors do not depend strongly on the difference between the nucleon and the Δ mass.

It is customary to quote the ratios of the electric and Coulomb quadrupole amplitudes to the magnetic dipole amplitude, R_{EM} (EMR) and R_{SM} (CMR). In the rest frame of the Δ , they are given by [46, 47]

$$\begin{aligned} R_{EM} &= -\frac{\mathcal{G}_{E2}(q^2)}{\mathcal{G}_{M1}(q^2)}, \\ R_{SM} &= -\frac{|\vec{q}|}{2m_\Delta} \frac{\mathcal{G}_{C2}(q^2)}{\mathcal{G}_{M1}(q^2)}. \end{aligned} \quad (7)$$

Deformation of the nucleon- Δ system will produce non-zero values of R_{EM} and R_{SM} . Using accurate measurements of the longitudinal-transverse response function at $q^2 = -0.127 \text{ GeV}^2$ it has been shown that a spherical nucleon - Δ system is inconsistent with the experimental results [12, 48].

III. LATTICE MATRIX ELEMENT

The most computationally demanding part in this evaluation is the calculation of the three-point correlation function given by

$$\langle G_\sigma^{\Delta j^\mu N}(t_2, t_1; \mathbf{p}', \mathbf{p}; \Gamma) \rangle = \sum_{\mathbf{x}_2, \mathbf{x}_1} \exp(-i\mathbf{p}' \cdot \mathbf{x}_2) \exp(+i(\mathbf{p}' - \mathbf{p}) \cdot \mathbf{x}_1) \Gamma^{\beta\alpha} \langle \Omega | T [\chi_\sigma^\alpha(\mathbf{x}_2, t_2) j^\mu(\mathbf{x}_1, t_1) \bar{\chi}^\beta(\mathbf{0}, 0)] | \Omega \rangle, \quad (8)$$

where an initial state with the quantum numbers of the nucleon is created at time zero and the final state with the quantum numbers of the Δ is annihilated at a later time t_2 . The photon couples to one of the quarks in the nucleon at an intermediate time t_1 producing a Δ . For the spin- $\frac{1}{2}$ source, $\chi^p(\mathbf{x}, t)$, and the spin- $\frac{3}{2}$ source, $\chi_\sigma^{\Delta^+}(\mathbf{x}, t)$, we use the interpolating fields

$$\chi^p(x) = \epsilon^{abc} [u^{T a}(x) C \gamma_5 d^b(x)] u^c(x) \quad , \quad (9)$$

$$\chi_\sigma^{\Delta^+}(x) = \frac{1}{\sqrt{3}} \epsilon^{abc} \left\{ 2 [u^{T a}(x) C \gamma_\sigma d^b(x)] u^c(x) + [u^{T a}(x) C \gamma_\sigma u^b(x)] d^c(x) \right\} \quad , \quad (10)$$

and for the projection matrices for the Dirac indices

$$\Gamma_i = \frac{1}{2} \begin{pmatrix} \sigma_i & 0 \\ 0 & 0 \end{pmatrix} \quad , \quad \Gamma_4 = \frac{1}{2} \begin{pmatrix} I & 0 \\ 0 & 0 \end{pmatrix} \quad . \quad (11)$$

For large Euclidean time separations $t_2 - t_1 \gg 1$ and $t_1 \gg 1$, the time dependence and field normalization constants cancel in the following ratio

$$R_\sigma(t_2, t_1, \mathbf{p}', \mathbf{p}, \Gamma, \mu) = \frac{G_\sigma^{\Delta j \mu N}(t_2, t_1, \mathbf{p}', \mathbf{p}, \Gamma)}{G_{ij}^{\Delta \Delta}(t_2, \mathbf{p}', \Gamma_4)} \left[\frac{G^{NN}(t_2 - t_1, \mathbf{p}, \Gamma_4) G_{ii}^{\Delta \Delta}(t_1, \mathbf{p}', \Gamma_4) G_{ii}^{\Delta \Delta}(t_2, \mathbf{p}', \Gamma_4)}{G_{ii}^{\Delta \Delta}(t_2 - t_1, \mathbf{p}', \Gamma_4) G^{NN}(t_1, \mathbf{p}, \Gamma_4) G^{NN}(t_2, \mathbf{p}, \Gamma_4)} \right]^{1/2} \\ \stackrel{t_2 - t_1 \gg 1}{\underset{t_1 \gg 1}{\longrightarrow}} \Pi_\sigma(\mathbf{p}', \mathbf{p}, \Gamma, \mu) \quad , \quad (12)$$

where G^{NN} and $G_{ij}^{\Delta \Delta}$ are the nucleon and Δ two-point functions given respectively by

$$\langle G^{NN}(t, \mathbf{p}; \Gamma) \rangle = \sum_{\mathbf{x}} e^{-i\mathbf{p} \cdot \mathbf{x}} \Gamma^{\beta\alpha} \langle \Omega | T \chi^\alpha(\mathbf{x}, t) \bar{\chi}^\beta(\mathbf{0}, 0) | \Omega \rangle \\ \langle G_{\sigma\tau}^{\Delta \Delta}(t, \mathbf{p}; \Gamma) \rangle = \sum_{\mathbf{x}} e^{-i\mathbf{p} \cdot \mathbf{x}} \Gamma^{\beta\alpha} \langle \Omega | T \chi_\sigma^\alpha(\mathbf{x}, t) \bar{\chi}_\tau^\beta(\mathbf{0}, 0) | \Omega \rangle \quad . \quad (13)$$

For the Wilson fermionic action we use the lattice conserved electromagnetic current, $j^\mu(x)$, given by

$$j_\mu(x) = \sum_f Q_f \kappa_f \{ \bar{\psi}^f(x + \hat{\mu})(1 + \gamma_\mu) U^{\mu\dagger}(x) \psi^f(x) - \bar{\psi}^f(x)(1 - \gamma_\mu) U^\mu(x) \psi^f(x + \hat{\mu}) \} \quad (14)$$

symmetrized on site x by taking $j^\mu(x) \rightarrow [j^\mu(x) + j^\mu(x - \hat{\mu})] / 2$, where Q_f is the charge of a quark of flavor f and κ_f is its hopping parameter. For domain wall fermions, we use the local four-dimensional electromagnetic current $\sum_f Q_f \{ \bar{\psi}^f(x) \gamma_\mu \psi^f(x) \}$. This is not conserved and therefore, to relate lattice and continuum results, we need the renormalization constants Z_V , which are known. Throughout this work we **choose** a frame where the Δ is at rest. For these kinematics we have $\mathbf{q} = -\mathbf{p}$, $\mathbf{p}' = \mathbf{0}$. At sufficiently large time separations, $t_2 - t_1$ and t_1 , R_σ becomes independent of time yielding the desired ratio Π_σ .

At the hadronic level, with the inclusion of complete sets of baryonic states and the use of Dirac and Rarita-Schwinger spinors the ratio of Eq. (12) leads to the relations

$$\Pi_\sigma(\mathbf{0}, -\mathbf{q}; \Gamma_4; \mu) = iA \epsilon^{\sigma 4 \mu j} p^j \mathcal{G}_{M1}(Q^2) \quad , \quad (15)$$

$$\Pi_\sigma(\mathbf{0}, -\mathbf{q}; \Gamma_k; j) = A \left\{ \frac{1}{2} (p_\sigma \delta_{kj} - p_k \delta_{\sigma j}) \mathcal{G}_{M1}(Q^2) - \left[\frac{3}{2} (p_\sigma \delta_{kj} + p_k \delta_{\sigma j}) - \frac{3p_\sigma p_k p_j}{\mathbf{p}^2} \right] \mathcal{G}_{E2}(Q^2) \right. \\ \left. - \frac{(E_N - m_\Delta)}{2m_\Delta} p_j \left(\delta_{\sigma k} - \frac{3p_\sigma p_k}{\mathbf{p}^2} \right) \mathcal{G}_{C2}(Q^2) \right\} \quad (16)$$

for $j = 1, 2, 3$ and

$$\Pi_\sigma(\mathbf{0}, -\mathbf{q}; \Gamma_k; 4) = iB \left(\delta_{\sigma k} - \frac{3p_\sigma p_k}{\mathbf{p}^2} \right) \mathcal{G}_{C2}(Q^2) \quad , \quad (17)$$

with the kinematical coefficients

$$A = \sqrt{\frac{2}{3}} \frac{m_\Delta + m_N}{4m_N E_N} \sqrt{\frac{E_N}{E_N + m_N}}, \quad B = \frac{\mathbf{p}^2}{2m_\Delta} A.$$

A convenient method for the evaluation of three-point functions is the *sequential inversion through the sink*. This requires fixing the hadronic state at t_2 to be the Δ with fixed vector index σ . The projection matrices Γ at the sink are also fixed, but the operator inserted at any time t_1 can be left arbitrary. Therefore, with one sequential inversion one can evaluate the three-point function for a large set of lattice momentum transfer values \mathbf{q} , any current direction μ and any operator insertions at any intermediate time t_1 . One then looks for a plateau as a function of t_1 that determines Π_σ . Eqs. (15-17) constitute a system of equations for the form factors \mathcal{G}_{M1} , \mathcal{G}_{E2} and \mathcal{G}_{C2} at each value of Q^2 . It must be noted that while three independent measurements of $\Pi_\sigma(\mathbf{q}; \Gamma; \mu)$ suffice for the determination of the form factors, increasing the combinations of μ and photon momentum \mathbf{q} which are measured improves the statistical accuracy of the form factors. With that goal in mind, we observe that Eqs. (15-17) are identically zero for several values of $\mathbf{q} = -\mathbf{p}$, e.g. Eq. (15) is zero when $j = \sigma$ or $j = \mu$. Furthermore, for a given selection of σ , not all lattice rotations of \mathbf{q} are giving non-zero contributions. We therefore search for the linear combinations of Eqs. (15-17) which maximize the number of non-zero \mathbf{q} contributions in a lattice rotationally invariant fashion and construct the following optimal combinations

$$S_1(\mathbf{q}; \mu) = \sum_{\sigma=1}^3 \Pi_\sigma(\mathbf{0}, -\mathbf{q}; \Gamma_4; \mu) = iA \left\{ (p_2 - p_3)\delta_{1,\mu} + (p_3 - p_1)\delta_{2,\mu} + (p_1 - p_2)\delta_{3,\mu} \right\} \mathcal{G}_{M1}(Q^2) \quad (18)$$

$$S_2(\mathbf{q}; \mu) = \sum_{\sigma \neq k=1}^3 \Pi_\sigma(\mathbf{0}, -\mathbf{q}; \Gamma_k; \mu) = -3A \left\{ ((p_2 + p_3)\delta_{1,\mu} + (p_3 + p_1)\delta_{2,\mu} + (p_1 + p_2)\delta_{3,\mu}) \mathcal{G}_{E2}(Q^2) \right. \\ \left. - 2 \frac{p_\mu}{\mathbf{p}^2} (p_1 p_2 + p_1 p_3 + p_2 p_3) \left[\mathcal{G}_{E2}(Q^2) + \frac{E_N - m_\Delta}{2m_\Delta} \mathcal{G}_{C2}(Q^2) \right] \right\}, \quad (19)$$

for $\mu = 1, 2, 3$. For $\mu = 4$ we have

$$S_2(\mathbf{q}; \mu = 4) = \frac{-i 6 B}{\mathbf{p}^2} (p_1 p_2 + p_1 p_3 + p_2 p_3) \mathcal{G}_{C2}(Q^2). \quad (20)$$

The three-point functions involved in S_1 and S_2 require one sequential inversion if one uses the appropriate linear combination directly in the construction of the Δ sink. Thus, with two inversions we obtain the maximal number of lattice determinations of the form factors for all the allowed lattice photon momenta \mathbf{q} . The S_1 -type matrix element determines \mathcal{G}_{M1} while the quadrupole form factors are extracted from the S_2 -type matrix element. The method is clearly superior to the method used in Refs. [40, 41] since the same CPU cost allows the evaluation of the form factors at all Q^2 . It should be noted that the evaluation using the S_2 -type sink does not determine \mathcal{G}_{C2} at the lowest allowed photon momentum $\mathbf{q} = (1, 0, 0) 2\pi/La$ (and at the equivalent momentum in the other two directions). For this reason we use, in addition, the combination

$$S_3(\mathbf{q}; \mu) = \Pi_3(\mathbf{0}, -\mathbf{q}; \Gamma_3; \mu) - (\Pi_1(\mathbf{0}, -\mathbf{q}; \Gamma_1; \mu) + \Pi_2(\mathbf{0}, -\mathbf{q}; \Gamma_2; \mu))/2 \quad (21)$$

to get \mathcal{G}_{C2} for the values of \mathbf{q} for which the S_2 -type sink vanishes. This linear combination gives

$$S_3(\mathbf{q}; \mu) = -\frac{3 A}{2} p_\mu \left[3 \left(\delta_{\mu,3} - \frac{p_3^2}{\mathbf{p}^2} \right) \mathcal{G}_{E2}(Q^2) + \frac{E_N - m_\Delta}{2m_\Delta} \left(1 - 3 \frac{p_3^2}{\mathbf{p}^2} \right) \mathcal{G}_{C2}(Q^2) \right] \quad (22)$$

for $\mu = 1, 2, 3$ and

$$S_3(\mathbf{q}; \mu = 4) = \frac{3 i B}{2} \left(1 - 3 \frac{p_3^2}{\mathbf{p}^2} \right) \mathcal{G}_{C2}(Q^2). \quad (23)$$

The full set of lattice measurements for the type S_1 , S_2 and S_3 matrix elements for all contributing values of μ and \mathbf{q} at a given Q^2 are analyzed simultaneously. We denote by $P(\mathbf{q}; \mu)$ the lattice measurements for the ratios R_σ using

Wilson fermions						
V	# of confs	κ	m_π (GeV)	m_π/m_ρ	m_N (GeV)	m_Δ (GeV)
Quenched, $\beta = 6.0$, $a^{-1} = 2.14(6)$ GeV						
$32^3 \times 64$	200	0.1554	0.563(4)	0.645(9)	1.267(11)	1.470(15)
$32^3 \times 64$	200	0.1558	0.490(4)	0.587(12)	1.190(13)	1.425(16)
$32^3 \times 64$	200	0.1562	0.411(4)	0.503(23)	1.109(13)	1.382(19)
		$\kappa_c = 0.1571$	0.	0.938(9)		
Unquenched, $\beta = 5.6$, $a^{-1} = 2.56(10)$ GeV						
$24^3 \times 40$	185 [51]	0.1575	0.691(8)	0.701(9)	1.485(18)	1.687(15)
$24^3 \times 40$	157 [51]	0.1580	0.509(8)	0.566(12)	1.280(26)	1.559(19)
$24^3 \times 32$	200 [52]	0.15825	0.384(8)	0.453(27)	1.083(18)	1.395(18)
		$\kappa_c = 0.1585$	0.	0.938(33)		

TABLE I: Parameters and number of gauge field configurations used in the calculation using Wilson fermions.

the three-point function constructed using the sink-types described in Eqs. (18-21) and with w_k their statistical error.

If we denote the solution vector by $F = \begin{pmatrix} \mathcal{G}_{M1} \\ \mathcal{G}_{E2} \\ \mathcal{G}_{C2} \end{pmatrix}$ we are led to the overcomplete set of equations

$$P(\mathbf{q}; \mu) = D(\mathbf{q}; \mu) \cdot F(Q^2). \quad (24)$$

The kinematical prefactors, $D(\mathbf{q}, \mu)$, are known analytically and we have inserted the continuum expressions as detailed in Eqs. (3) and (4). As already pointed out, we have lattice measurements for all possible vector current components μ and photon momentum vectors q which contribute to a given value of Q^2 . For N such measurements, the matrix $D(\mathbf{q}; \mu)$ is an $N \times 3$ matrix of kinematical coefficients. The solution vector is determined from the minimization of the total χ^2

$$\chi^2 = \sum_{k=1}^N \left(\frac{\sum_{j=1}^3 D_{kj} F_j - P_k}{w_k} \right)^2. \quad (25)$$

Defining $D'_{kj} = D_{kj}/w_k$ and $P'_k = P_k/w_k$, ($k = 1, 2, \dots, N, j = 1, 2, 3$) the solution is obtained using the singular value decomposition of the matrix $D'_{kj}(\mathbf{q}; \mu)$

$$D' = U \cdot \text{diag}(\lambda_1, \lambda_2, \lambda_3) \cdot V^T, \quad (26)$$

where U is an $N \times 3$ matrix, V is a 3×3 matrix and the λ_j are the non-negative, singular values of D' . The form factors are therefore given by

$$F = V \cdot \text{diag}(1/\lambda_1, 1/\lambda_2, 1/\lambda_3) \cdot (U^T \cdot P'). \quad (27)$$

This strategy has been developed in [49] and also applied in [50] and subsequent publications. The errors w_k in the lattice measurements and the final error on the form factors are determined from the jackknife procedure. Having decided to use sequential inversions through the sink, the sink-source separation must be kept fixed. One would like to use the smallest sink-source separation that guarantees that excited state contributions are negligible. In our previous work we found that a sink-source separation, t_2 , of about 5 GeV^{-1} is sufficient. We check in the next Section that this is also sufficient for this calculation by comparing to the results obtained when we increase t_2 by about 25%.

In the hybrid action approach we have applied hypercubic (HYP)-smearing [53] to the gauge fields. We have performed the computation using two different boundary conditions (b.c.) in the temporal direction. In the first case we impose Dirichlet b.c. on time slices 0 and 31 using only the first half of the lattice and in the second we use the full lattice with antiperiodic b.c. consistent with the b.c. used in the production of the gauge fields. The lattice spacing $a = 0.1241 \text{ fm}$ has been determined from heavy-quark spectroscopy [54] with a statistical uncertainty of 2%. For Wilson fermions we use antiperiodic b.c.

To improve convergence to the nucleon and Δ ground states we use Gaussian or Wuppertal smearing to create smeared quark fields as described in Refs. [36, 55] with smearing parameters $\alpha = 4$ and $n = 50$.

The parameters and number of gauge field configurations are summarized in Table I for Wilson fermions and in Table II for the hybrid action.

V	# of confs	$L_S m_\pi$ (fm)	$(am_{u,d/s})^{\text{Asqtad}}$	$(am_{u,d})^{\text{DWF}}$	m_π (GeV)	m_π/m_ρ	m_N (GeV)	m_Δ (GeV)
$20^3 \times 32$	150	2.5	0.03/0.05	0.0478	0.606(2)	0.588(7)	1.329(9)	1.662(21)
$20^3 \times 32$	150	2.5	0.02/0.05	0.0313	0.502(4)	0.530(11)	1.255(19)	1.586(36)
$28^3 \times 32$	118	3.5	0.01/0.05	0.0138	0.364(1)	0.387(7)	1.196(25)	1.561(41)
$20^3 \times 64$	200	2.5	0.03/0.05	0.0478	0.594(1)	0.585(7)	1.416(20)	1.683(22)
$20^3 \times 64$	198	2.5	0.02/0.05	0.0313	0.498(3)	0.525(8)	1.261(17)	1.589(35)
$20^3 \times 64$	100	2.5	0.01/0.05	0.0138	0.362(5)	0.401(13)	1.139(25)	1.488(71)
$28^3 \times 64$	300	3.5	0.01/0.05	0.0138	0.353(2)	0.368(8)	1.191(19)	1.533(27)

TABLE II: Parameters and number of gauge field configurations used for the hybrid action.

Domain wall fermions (DWF) [56, 57, 58] introduce an additional fifth dimension of length L_5 . They preserve the Ward-Takahashi identity [59] even at finite lattice spacing in the limit $L_5 \rightarrow \infty$. At sufficiently small values of the lattice spacing a , the effect of a finite value of L_5 can be parameterized by an additional residual mass term in the Ward-Takahashi identity [60, 61]. This behavior describes a residual explicit breaking of chiral symmetry which can be minimized by choosing a sufficiently large extra dimension, L_5 . We have found that a value of $L_5 = 16$ in lattice units is sufficient to keep the residual mass, $(am)_{\text{res}}$, at most one order of magnitude smaller than the domain wall quark mass, $(am)_q^{\text{DWF}}$. The height parameter of the domain wall action has been chosen to be $am_0 = 1.7$.

The DWF quark masses displayed in Tables II have been tuned by adjusting the lightest pseudoscalar meson in the Asqtad calculation [27] to have the same mass as the pseudoscalar meson using domain-wall fermions. For technical details of this tuning procedure, see [29, 34].

IV. EXTRACTION OF FORM FACTORS FROM LATTICE RESULTS

In this section we discuss several technical issues, beyond the general methodology described in the previous section, that must be addressed before the N to Δ form factors can be extracted reliably from lattice measurements.

As mentioned already, given that sequential inversions are the most time consuming part of the calculation, the method of choice to calculate form factors that are functions of the momentum transfer squared is to perform sequential inversions through the sink. However, this approach requires that we fix the initial and final hadron states as well as the sink-source time separation, t_2 . Changing t_2 requires a new sequential inversion.

Therefore we must first determine the optimal value of t_2 . The criterion is to choose t_2 as small as possible so that statistical errors due to the exponential decrease of the signal are minimized but large enough so that we ensure that excited states with the nucleon and Δ quantum numbers are suppressed. In order to decide on the value of t_2 we compare results at two different sink-source separations in the quenched theory and in the hybrid approach. The quenched theory is used to provide a guideline because the statistical errors are the smallest and therefore deviations due to contamination from excited states can be seen more easily. We use two time separations, namely $t_2/a = 11$ and 13 and perform the calculation at the smallest pion mass. In Fig. 1 we show results for the ratio R_{S_1} defined as in Eq. (12) but using the optimal source of Eq. (18) for the three-point function and normalized with the appropriate kinematical factors such that the plateau value yields \mathcal{G}_{M1} . Note that this is not what is actually done in the overconstrained analysis where the plateau value for each value of the momentum vector is extracted. Nevertheless R_{S_1} shown in Fig. 1 gives an idea of the quality of the plateaus that are obtained. We show results for the four lowest Q^2 -values when the sink-source separation is taken $t_2/a = 11$. We compare the results obtained for sink-source separation $t_2/a = 13$ at the two lowest Q^2 values and at the largest value shown in the figure. The third lowest Q^2 value corresponding to $n^2 = 3$ for $t_2/a = 13$ is not included since it will make the figure difficult to read. As can be seen the two time separations yield consistent results over a time range t_1 . Although in this comparison we use the same number of configurations the statistical errors are much smaller for the shorter time separation. Fitting to a constant over the plateau range but now for individual momentum vectors within the overconstrained analysis we obtained \mathcal{G}_{M1} . The results are shown in Fig. 1, for the two different time separations using 100 configurations in each case. As can be seen there is very good agreement showing that a time separation of about 5 GeV^{-1} is sufficient.

It is important to ensure that what we find in the quenched case carries over to the hybrid action. We expect pion cloud effects to be important for dynamical quarks and therefore we must check that the time evolution is large enough to allow the pion cloud to fully develop. Guided by our findings in the quenched theory we choose $t_2/a = 8$ or about 5 GeV^{-1} and $t_2/a = 10$ or about 6.3 GeV^{-1} . In Fig. 2 we show the ratio R_{S_1} for the two heaviest quark masses whereas in Fig. 3 we show the results for \mathcal{G}_{M1} at the smallest quark mass for the two different time separations. As can be seen, R_{S_1} at the two lowest Q^2 values yields the same plateau value for both time separations. For $t_2/a = 10$ the statistical errors are larger associated with the larger time separation. The values extracted for \mathcal{G}_{M1} at the smallest

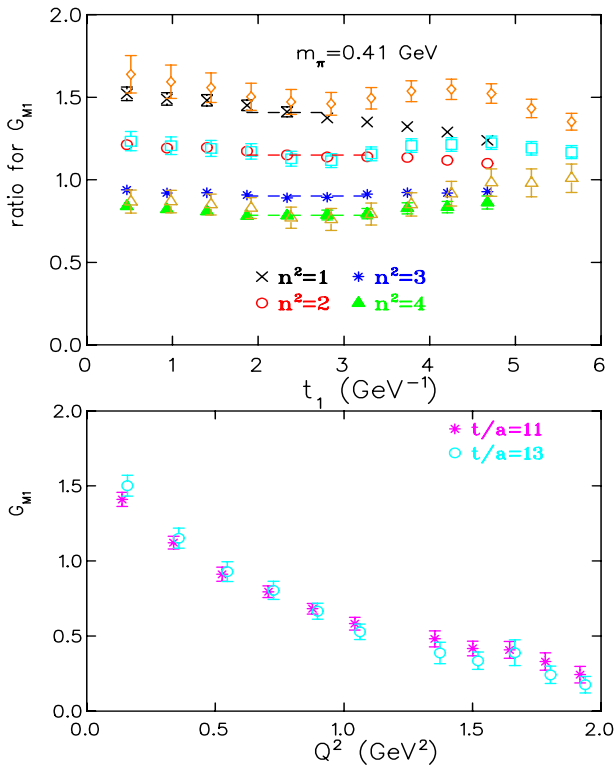


FIG. 1: Upper graph: The ratio from which \mathcal{G}_{M1} is extracted as a function of time separation for the four lowest Q^2 -values taking the sink-source separation $t_2 = 11a$ in the quenched theory at pion mass $m_\pi = 411$ MeV. We also show results obtained with sink-source separation $t_2 = 13a$, at the two lowest values of Q^2 (rhombus and open squares respectively) and at the fourth lowest (open triangles), displaced to the left for clarity. The dashed lines are fits to the plateaus obtained with $t_2 = 11a$ and span the range of fitted points. The lower graph shows \mathcal{G}_{M1} at $m_\pi = 411$ MeV, for sink-source separations $t_2 = 11a$ (asterisks) and $t_2 = 13a$ (open circles), displaced to the right, for clarity.

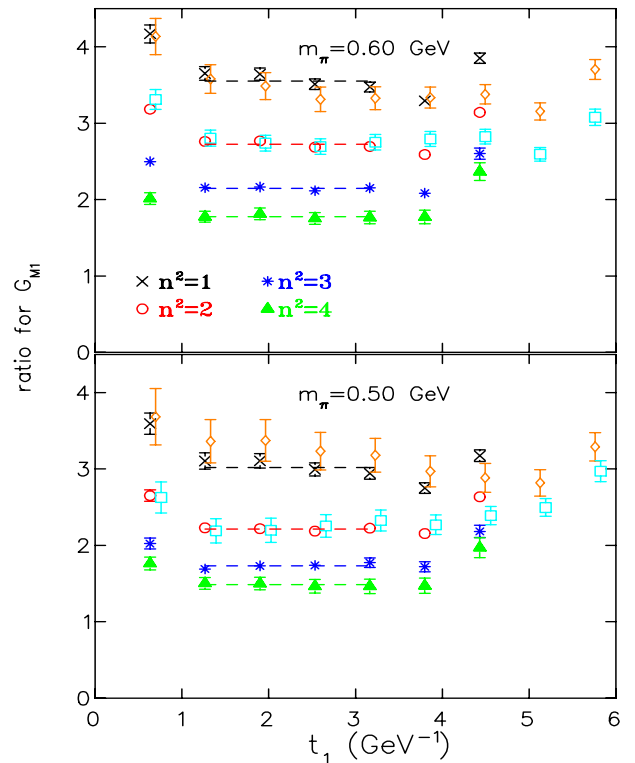


FIG. 2: The ratio from which \mathcal{G}_{M1} is extracted for the hybrid action using a spatial volume 20^3 as function of time separation. We show results for the four lowest Q^2 -values taking the sink-source separation $t_2 = 8a$. For the two lowest values of Q^2 , we show results obtained with sink-source separation $t_2 = 10a$ (rhombus for lowest and open squares for second lowest momentum), displaced to the right, for clarity. The upper graph is for $m_\pi = 0.594(1)$ GeV and the lower for $m_\pi = 0.498(2)$ GeV. The dashed lines are fits to the plateaus obtained with $t_2 = 8a$ and span the range of fitted points.

pion mass, where pion cloud effects are expected to be the largest, are also consistent for the two time separations, as can be seen in Fig. 3. The deviations observed at $Q^2 > 1.5$ are due to the large statistical noise associated with the larger time evolution. We therefore conclude from this analysis that a time separation of about 5 GeV^{-1} is also sufficient for our unquenched study. As a result we fix $t_2 \sim 5 \text{ GeV}^{-1}$ or in lattice units to 11 in the quenched case, to 12 for $N_F = 2$ dynamical Wilson fermions and to 8 in the hybrid approach.

Another potential source of a systematic error is the spatial size of our lattices. Given that for the quenched case we use a lattice of spatial size of about 3 fm we expect finite volume effects to be negligible. Since we do not have dynamical Wilson configurations on a larger volume we test for finite size effects in the hybrid scheme for which, at the smallest quark mass, there are MILC configurations for spatial lattice size $L_s = 2.5$ fm and $L_s = 3.5$ fm giving $L_s m_\pi = 4.6$ and $L_s m_\pi = 6.4$, respectively. In Fig. 4 we show results for \mathcal{G}_{M1} for these two spatial sizes. Results on the smaller lattice are consistent with results on the larger lattice. This indeed shows that finite volume effects are small for $L_s m_\pi \gtrsim 4.5$. Since for all our quark masses, except the lightest mass dynamical Wilson fermions $L_s m_\pi > 4.6$, we expect finite volume effects to be small.

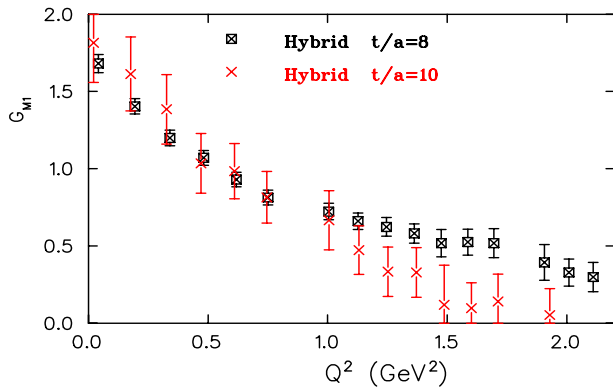


FIG. 3: \mathcal{G}_{M1} as function of Q^2 at the lowest quark mass for the hybrid action for sink-source separations $t_2/a = 8$ and $t_2/a = 10$.

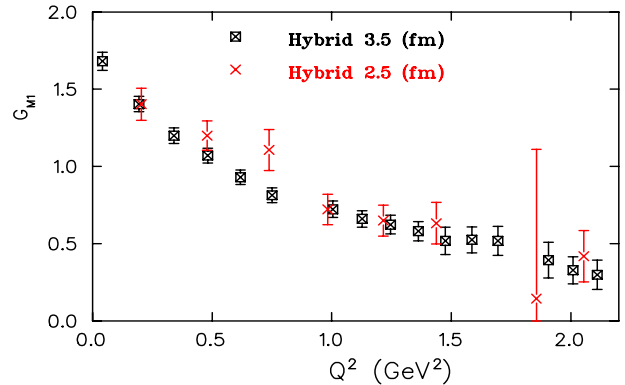


FIG. 4: \mathcal{G}_{M1} as function of Q^2 at the lowest quark mass for the hybrid action for spatial volume 20^3 and 28^3 .

V. RESULTS FOR THE NUCLEON TO Δ TRANSITION FORM FACTORS

The lattice results for the dominant dipole form factor are shown in Fig. 5 as we change the quark mass in the three types of simulations considered in this work, namely in the quenched theory denoted by $N_F = 0$, for two degenerate flavors of dynamical Wilson fermions, denoted by $N_F = 2$ and in the hybrid scheme. They are also given in Tables III, IV and V of the Appendix. All the results discussed in this section in the hybrid approach are obtained on the lattices of temporal extent 64 and using antiperiodic boundary conditions in the temporal direction.

In all three cases the magnetic dipole decreases with the quark mass. The dashed lines are fits to an exponential Ansatz $f_0 \exp(-Q^2/m^2)$ whereas the dotted lines to a dipole Ansatz $g_0/(1 + Q^2/m_0^2)$ at the lightest quark mass. As can be seen, both provide a good description to the lattice results. The dipole mass that we find in the hybrid approach at the smallest pion mass is $m_0 = 1.30(3)$ GeV. For comparison, a dipole fit to the experimental results yields $m_0 = 0.78$ GeV reflecting the faster fall off of the experimental results. In Fig. 6 we compare quenched and unquenched results for \mathcal{G}_{M1} at the three quark masses. For similar pion mass the results are in agreement even for pion mass as low as 350 MeV. As can be seen, lattice results fall approximately on the same curve having a weaker Q^2 dependence than the experimental results. In the momentum range considered here experimental results can be well described by a dipole form. In fact, whereas the experimental results fall off faster than the dipole form factor of the nucleon $G_D = 1/(1 + Q^2/0.71)^2$ with $m_0 = 0.78 < \sqrt{0.71}$, the lattice results display a weaker Q^2 dependence yielding larger values for m_0 . It remains an open question whether decreasing the quark mass towards the physical limit will modify this Q^2 dependence.

In Figs. 7 and 8 we show the results for the EMR and CMR ratios at the lightest quark mass, whereas we give the complete set of numbers in Tables III, IV and V. In the case of Wilson fermions we use both sink types S_2 and S_3 to extract $\mathcal{G}_{E2}(Q^2)$ and $\mathcal{G}_{C2}(Q^2)$. For domain wall fermions, for which inversions are very expensive, we only use S_2 , which means that $\mathcal{G}_{C2}(Q^2)$ is not determined at the lowest momentum transfer as well as at some intermediate values. However, we obtain results at the second lowest momentum transfer squared which for the lowest pion mass on the 28^3 lattice is about the same as the lowest momentum on our quenched lattice, enabling a nice comparison. The main conclusion of this study is that these ratios are non-zero and negative. As can be seen in Fig. 7, there is agreement between the quenched results for EMR and those obtained within the hybrid approach at the smallest quark mass. For the CMR ratio there is a notable difference: At the lowest value of Q^2 the quenched results yield a value that is clearly negative but smaller in magnitude than experiment. Results in the hybrid approach at the smallest quark mass are negative and larger in magnitude decreasing the gap between the lattice value and experiment. This confirms that pion cloud contributions are significant at small Q^2 modifying the quenched results. This is consistent with the expectation from chiral perturbation theory [44] that pion cloud contributions become significant at low Q^2 . Large pion contributions are also needed in phenomenological approaches [66, 67, 69].

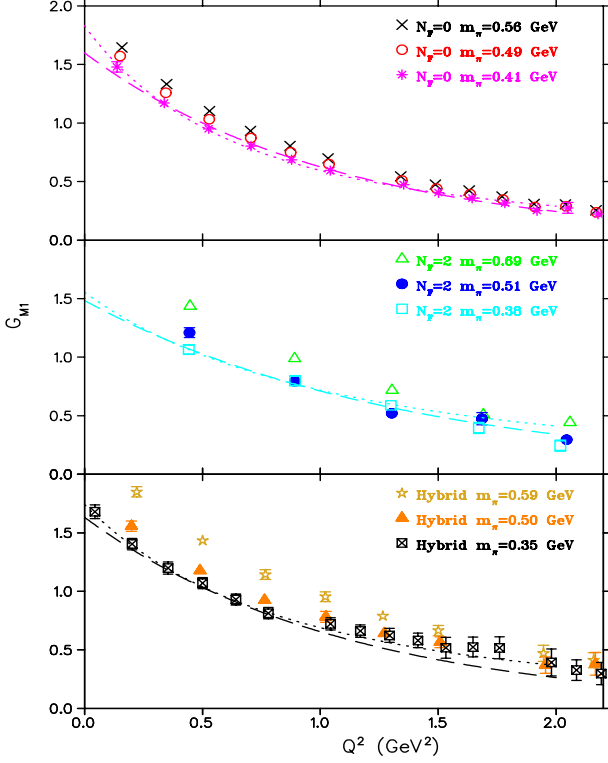


FIG. 5: The dipole form factor \mathcal{G}_{M1} as a function of Q^2 . The upper graph is for the quenched theory where results at $m_\pi = 563$ MeV are denoted by the crosses, at $m_\pi = 490$ MeV by the open circles and at $m_\pi = 411$ MeV by the asterisks. The middle graph is for dynamical Wilson fermions where results at $m_\pi = 691$ MeV are denoted by the open triangles, at $m_\pi = 509$ MeV by the filled circles and at $m_\pi = 384$ MeV by the open squares. The lower is for the hybrid action, where results at $m_\pi = 594$ MeV are denoted by the stars, at $m_\pi = 498$ MeV by the filled triangles and at $m_\pi = 353$ MeV by the inscribed squares. The dashed line is a fit to an exponential form $f_0 \exp(-Q^2/m^2)$ and the dotted line is a fit to a dipole form $g_0/(1+Q^2/m_0^2)^2$ at the lowest pion mass in each of the three types of simulations.

VI. CONCLUSIONS

We have presented results for the N to Δ electromagnetic transition form factors calculated within full QCD, using two degenerate flavors of dynamical Wilson fermions, and using a hybrid action with staggered sea quarks and domain wall valence quarks. Comparison of these results with previous quenched calculations [16] do not reveal large unquenching effects in the case of the dominant dipole form factor, \mathcal{G}_{M1} , for pion masses down to about 350 MeV. All lattice results for \mathcal{G}_{M1} at these quark masses show a weaker Q^2 dependence than experiment. Comparison of results with the hybrid action at two different volumes indicates that volume effects are not larger than our statistical errors. Therefore we can not attribute this weaker Q^2 dependence to finite volume effects. Agreement between results using dynamical Wilson fermions and Domain Wall fermions that have different finite lattice spacing systematics suggests that it is unlikely to be due to discretization errors. However, we cannot presently extrapolate the lattice results to the continuum limit. Such an extrapolation would require three different lattice spacings at similar volumes and quark masses, which are currently not available. For the EMR and CMR ratios, on the other hand, unquenched lattice results begin to show agreement with experiment. One of the main results of this study is the quark mass dependence of the CMR ratio at low Q^2 . Whereas quenched lattice results underestimate the magnitude of CMR at low Q^2 , results in full QCD become more negative, bringing lattice results closer to experiment. This demonstrates the importance of

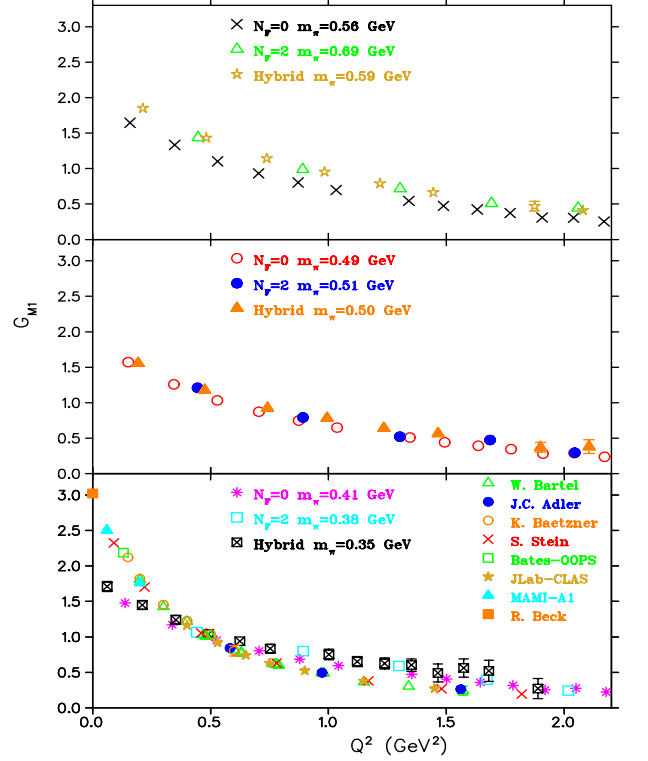


FIG. 6: The dipole form factor \mathcal{G}_{M1} as a function of Q^2 . The upper graph is for the heaviest quark mass, the middle graph for the intermediate quark mass and the lower for the lightest quark mass for the three type of simulations considered in this work. The notation for the lattice results is the same as that in Fig. 5. The lattice results at the smallest pion mass (lower graph) are compared to experiment where open triangles are results from Ref. [62], filled circles from Ref. [63], open circles from Ref. [64], crosses from Ref. [65], open squares from Ref. [9], stars from Refs. [11, 66, 67], filled triangles from Refs. [13, 14] and the filled square at $Q^2 = 0$ from Ref. [8].

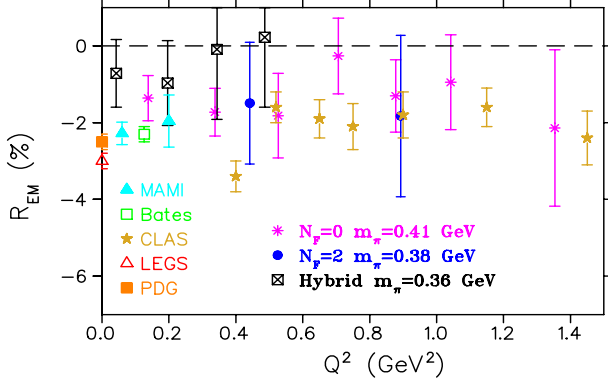


FIG. 7: Lattice calculations of EMR, denoted by R_{EM} , for the lightest quark mass with each action. We include experimental results on EMR from Refs. [13, 14] (filled triangles), [9] (open square), [11] (stars), [7] (open triangle) and [68] (filled square).

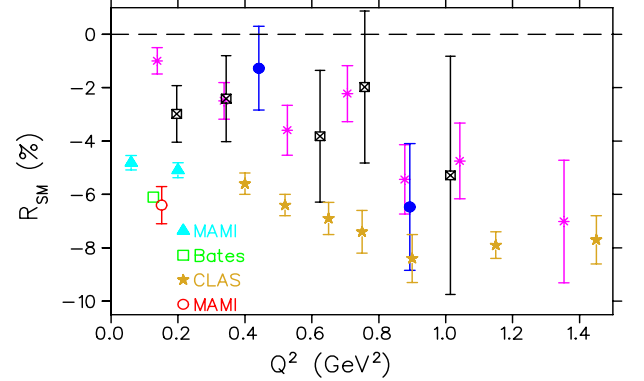


FIG. 8: Lattice calculations of CMR for the lightest quark mass with each action. We include experimental results on CMR. The notation is the same as that of Fig. 7. The open circle shows the result from Ref. [10].

full QCD dynamics in the quadrupole form factors as one enters the chiral regime.

The largest conceptual question as we enter the chiral regime in full QCD, is how to fully incorporate the physical effect of the decay of the Δ into a pion and nucleon on the transition form factors. Even when the pion is sufficiently light that the Δ could decay in an infinite box, the p -wave pion in a small box can still be above the decay threshold. Naive extrapolation to the chiral limit without including the decay threshold could produce qualitative errors in form factors, such as the discrepancy presently observed between the lattice and experimental magnetic form factors. In the event that chiral perturbation theory is sufficiently accurate at and above the Δ decay threshold, finite volume chiral perturbation theory would be an attractive framework for addressing decay channel physics. Otherwise, extension of finite volume techniques presently used for phase shifts will be required to address form factors. This presents an exciting and important research challenge.

Acknowledgments

We would like to thank B. Orth, Th. Lippert and K. Schilling [51] as well as C. Urbach, K. Jansen, A. Shindler and U. Wenger [52] and the MILC collaboration for providing the unquenched configurations used in this work, as well as the LHP collaboration for providing forward propagators [29]. A.T. would like to acknowledge support by the University of Cyprus and the program “Pythagoras” of the Greek Ministry of Education and G. K. by the Cyprus Research Promotion Foundation. This work is supported in part by the EU Integrated Infrastructure Hadron Physics (I3HP) under contract RII3-CT-2004-506078, by the DFG (Forschergruppe Gitter-Hadronen-Phänomenologie), by the U.S. Department of Energy (D.O.E.) Office of Nuclear Physics under contract DE-FG02-94ER40818 and by the National Science Council of Taiwan under the grant numbers NSC96-2112-M002-020-MY3 and NSC96-2811-M002-026.

This research used computational resources provided by the IBM machine at NIC, Jülich, Germany, by the National Energy Research Scientific Computing Center, which is supported by the Office of Science of the U.S. Department of Energy under Contract No. DE-AC03-76SF00098, and by the MIT Blue Gene computer, supported by the DOE under grant DE-FG02-05ER25681.

-
- [1] N. Isgur, G. Karl, and R. Koniuk, Phys.Rev. **D25**, 2394 (1982).
 - [2] S. Capstick and G. Karl, Phys.Rev. **D41**, 2767 (1990).
 - [3] A. Bohr and B. Mottelson, *Nuclear Structure II* (Benjamin, Reading, MA, 1975).
 - [4] C. Alexandrou, P. de Forcrand, and A. Tsapalis, Phys. Rev. **D66**, 094503 (2002), hep-lat/0206026.
 - [5] C. Alexandrou, Nucl. Phys. Proc. Suppl. **128**, 1 (2004), hep-lat/0311007.
 - [6] C. Alexandrou, T. Korzec, T. Leontiou, J. W. Negele, and A. Tsapalis, PoS **LAT2007**, 149 (2007), arXiv:0710.
 - [7] G. Blanpied et al. (LEGS), Phys. Rev. Lett. **76**, 1023 (1996).
 - [8] R. Beck et al., Phys. Rev. **C61**, 035204 (2000), nucl-ex/9908017.
 - [9] C. Mertz et al. (OOPS), Phys. Rev. Lett. **86**, 2963 (2001), nucl-ex/9902012.

- [10] T. Pospischil et al., Phys. Rev. Lett. **86**, 2959 (2001).
- [11] K. Joo et al. (CLAS), Phys. Rev. Lett. **88**, 122001 (2002), hep-ex/0110007.
- [12] N. F. Sparveris et al., Phys. Rev. Lett. **94**, 022003 (2005), nucl-ex/0408003.
- [13] S. Stave et al. (OOPS), Eur. Phys. J. **A30**, 471 (2006), nucl-ex/0604013.
- [14] N. F. Sparveris et al., Phys. Lett. **B651**, 102 (2007), nucl-ex/0611033.
- [15] A. M. Bernstein and C. N. Papanicolas, AIP Conference Proceedings **104**, 1 (2007).
- [16] C. Alexandrou et al., Phys. Rev. Lett. **94**, 021601 (2005), hep-lat/0409122.
- [17] C. Alexandrou et al., Nucl. Phys. Proc. Suppl. **140**, 293 (2005), hep-lat/0408017.
- [18] C. Alexandrou et al., PoS **LAT2005**, 091 (2006), hep-lat/0509140.
- [19] M. Vanderhaeghen, AIP Conf. Proc. **904**, 25 (2007).
- [20] T. A. Gail and T. R. Hemmert, AIP Conf. Proc. **904**, 151 (2007).
- [21] C. Alexandrou, P. de Forcrand, and A. Tsapalis, Phys. Rev. **D68**, 074504 (2003), hep-lat/0307009.
- [22] C. Alexandrou, P. de Forcrand, and A. Tsapalis, Nucl.Phys.Proc.Suppl. **129**, 221 (2004), hep-lat/0309064.
- [23] C. Alexandrou and G. Koutsou, PoS **LAT2007**, 150 (2007), arXiv:0710.2441.
- [24] C. Alexandrou, P. Dimopoulos, G. Koutsou, and H. Neff, PoS **LAT2005**, 030 (2006), hep-lat/0509125.
- [25] C. Alexandrou, G. Koutsou, and H. Neff, PoS **LAT2006**, 113 (2006), hep-lat/0610039.
- [26] C. Alexandrou, AIP Conf.Proc. **904**, 49 (2007), hep-lat/0608007.
- [27] C. W. Bernard et al., Phys. Rev. **D64**, 054506 (2001), hep-lat/0104002.
- [28] J. W. Negele et al., Nucl. Phys. Proc. Suppl. **128**, 170 (2004), hep-lat/0404005.
- [29] D. B. Renner et al. (LHPC), Nucl. Phys. Proc. Suppl. **140**, 255 (2005), hep-lat/0409130.
- [30] P. Hägler et al. (LHPC), Eur. Phys. J. **A24S1**, 29 (2005), hep-ph/0410017.
- [31] R. G. Edwards et al. (LHPC), Phys. Rev. Lett. **96**, 052001 (2006), hep-lat/0510062.
- [32] R. G. Edwards et al. (LHPC), PoS **LAT2005**, 056 (2006), hep-lat/0509185.
- [33] R. G. Edwards et al. (2006), hep-lat/0610007.
- [34] P. Hägler et al. (LHP) (2007), arXiv:0705.4295.
- [35] C. Alexandrou, T. Leontiou, J. W. Negele, and A. Tsapalis, Phys. Rev. Lett. **98**, 052003 (2007), hep-lat/0607030.
- [36] C. Alexandrou, G. Koutsou, T. Leontiou, J. W. Negele, and A. Tsapalis, Phys. Rev. D (**in press**) (2007), arXiv:0706.3011.
- [37] C. Alexandrou, T. Leontiou, J. W. Negele, and A. Tsapalis, PoS **LAT2006**, 115 (2006), hep-lat/0610107.
- [38] C. Alexandrou, G. Koutsou, T. Leontiou, J. W. Negele, and A. Tsapalis, PoS **LAT2007**, 162 (2007), arXiv:0710.2173.
- [39] C. Alexandrou, World Scientific (2007), arXiv:0710.1202.
- [40] D. B. Leinweber, T. Draper, and R. M. Woloshyn, Phys. Rev. **D48**, 2230 (1993), hep-lat/9212016.
- [41] C. Alexandrou et al., Phys. Rev. **D69**, 114506 (2004), hep-lat/0307018.
- [42] C. Alexandrou et al., Nucl. Phys. Proc. Suppl. **129**, 302 (2004), hep-lat/0309041.
- [43] W. Schroers (2007), hep-lat/0701003.
- [44] V. Pascalutsa and M. Vanderhaeghen, Phys. Rev. Lett. **95**, 232001 (2005), hep-ph/0508060.
- [45] A. A. Khan et al., Phys. Rev. **D74**, 094508 (2006), hep-lat/0603028.
- [46] H. F. Jones and M. C. Scadron, Ann. Phy (N.Y.) **81**, 1 (1973).
- [47] G. C. Gellas, T. R. Hemmert, C. N. Ktorides, and G. I. Poulis, Phys. Rev. **D60**, 054022 (1999), hep-ex/0110007.
- [48] C. N. Papanicolas, Eur. Phys. J. **A18**, 141 (2003).
- [49] P. Hägler et al. (LHPC), Phys. Rev. **D68**, 034505 (2003), hep-lat/0304018.
- [50] M. Göckeler et al. (QCDSF), Phys. Rev. Lett. **92**, 042002 (2004), hep-ph/0304249.
- [51] O. Orth, T. Lippert, and K. Schilling (T χ L), Phys. Rev. D **72**, 014503 (2005).
- [52] C. Urbach et al., Comput. Phys. Commun. **174**, 87 (2006).
- [53] A. Hasenfratz and F. Knechtli, Phys. Rev. **D64**, 034504 (2001), hep-lat/0103029.
- [54] C. Aubin et al., Phys. Rev. **D70**, 094505 (2004), hep-lat/0402030.
- [55] C. Alexandrou, G. Koutsou, J. W. Negele, and A. Tsapalis, Phys. Rev. **D74**, 034508 (2006), hep-lat/0605017.
- [56] D. B. Kaplan, Phys. Lett. **B288**, 342 (1992), hep-lat/9206013.
- [57] Y. Shamir, Nucl. Phys. **B406**, 90 (1993), hep-lat/9303005.
- [58] R. Narayanan and H. Neuberger, Phys. Lett. **B302**, 62 (1993), hep-lat/9212019.
- [59] V. Furman and Y. Shamir, Nucl. Phys. **B439**, 54 (1995), hep-lat/9405004.
- [60] T. Blum et al., Phys. Rev. **D69**, 074502 (2004), hep-lat/0007038.
- [61] T. Blum, Nucl. Phys. Proc. Suppl. **73**, 167 (1999), hep-lat/9810017.
- [62] W. Bartel et al., Phys. Lett. **B28**, 148 (1968).
- [63] J. C. Alder et al., Nucl. Phys. **B46**, 573 (1972).
- [64] K. Bätzner et al., Phys. Lett. **B39**, 575 (1972).
- [65] S. Stein et al., Phys. Rev. **D12**, 1884 (1975).
- [66] L. Tiator et al., Nucl. Phys. A **689**, 205 (2001), nucl-th/0012046.
- [67] L. Tiator, D. Drechsel, S. S. Kamalov, and S. N. Yang, Eur. Phys. J. A **17**, 357 (2003).
- [68] K. Hagiwara et al. (Particle Data Group), Phys. Rev. **D66**, 010001 (2002).
- [69] T. Sato and T.-S. H. Lee, Phys. Rev. C **63**, 055201 (2001).

VII. APPENDIX

Wilson fermions			
Q^2 (GeV ²)	\mathcal{G}_{M1}	EMR %	CMR %
Quenched, $\beta = 6.0$, $a^{-1} = 2.14(6)$ GeV			
$m_\pi = 563(4)$ MeV			
0.158	1.646(30)	-0.72(26)	-0.82(26)
0.348	1.332(23)	-0.86(29)	-2.09(39)
0.530	1.102(29)	-0.60(57)	-2.62(52)
0.704	0.933(22)	-0.51(47)	-1.80(60)
0.871	0.804(22)	-0.82(45)	-3.11(77)
1.033	0.698(23)	-0.62(63)	-2.92(84)
1.341	0.545(25)	-1.33(93)	-4.31(1.21)
1.488	0.474(24)		
1.631	0.424(26)		
1.770	0.373(25)		
1.906	0.309(28)		
2.039	0.306(34)		
2.169	0.254(28)		
2.420	0.202(52)		
$m_\pi = 490(4)$ MeV			
0.151	1.572(33)	-0.93(36)	-0.92(33)
0.344	1.259(31)	-1.18(38)	-2.33(48)
0.529	1.033(30)	-1.03(76)	-2.99(66)
0.705	0.873(26)	-0.47(64)	-1.97(74)
0.874	0.749(24)	-1.05(62)	-3.87(93)
1.037	0.649(25)	-0.79(83)	-3.46(1.04)
1.346	0.510(28)	-1.65(1.28)	-5.44(1.54)
1.493	0.441(25)		
1.636	0.393(28)		
1.775	0.346(28)		
1.910	0.283(31)		
2.042	0.290(38)		
2.171	0.238(30)		
2.420	0.185(52)		
$m_\pi = 411(4)$ MeV			
0.138	1.479(44)	-1.36(59)	-0.99(50)
0.338	1.171(37)	-1.73(62)	-2.49(69)
0.527	0.951(35)	-1.82(1.10)	-3.59(93)
0.706	0.804(32)	-0.26(99)	-2.22(1.05)
0.878	0.687(26)	-1.30(94)	-5.44(1.30)
1.042	0.595(29)	-0.95(1.24)	-4.74(1.42)
1.353	0.475(34)	-2.14(2.04)	-7.01(1.22)
1.501	0.406(28)		
1.644	0.359(30)		
1.783	0.317(31)		
1.918	0.252(35)		
2.050	0.276(45)		
2.178	0.223(34)		
2.426	0.172(57)		

TABLE III: Quenched results for \mathcal{G}_{M1} , EMR and CMR

Wilson fermions			
Q^2 (GeV ²)	\mathcal{G}_{M1}	EMR %	CMR %
$N_F = 2$ Wilson, $\beta = 5.6$, $a^{-1} = 2.56(10)$ GeV			
$m_\pi = 691(8)$			
0.447	1.437(36)	-0.76(43)	-1.76(69)
0.891	0.989(31)	-0.86(71)	-3.03(1.04)
1.304	0.717(30)	-1.44(1.33)	-0.88(1.34)
1.691	0.509(40)	-2.28(1.42)	-5.75(1.95)
2.058	0.443(38)	-2.08(1.48)	-10.06(2.41)
2.407	0.341(37)		
3.060	0.208(55)		
$m_\pi = 509(8)$			
0.445	1.210(42)	-1.00(1.28)	-0.93(1.42)
0.892	0.794(32)	-5.26(1.87)	-6.17(2.10)
1.303	0.521(32)	-5.95(4.43)	-3.49(3.44)
1.685	0.474(52)	-5.65(3.47)	-4.02(3.33)
2.044	0.296(32)		
2.384	0.211(48)		
$m_\pi = 384(8)$			
0.442	1.066(43)	-1.49(1.59)	-1.27(1.57)
0.893	0.798(44)	-1.83(2.10)	-6.47(2.37)
1.299	0.589(37)		
1.671	0.396(48)		
2.017	0.244(47)		
2.342	0.181(41)		

TABLE IV: Unquenched Wilson results for \mathcal{G}_{M1} , EMR and CMR.

Hybrid action			
Q^2 (GeV ²)	\mathcal{G}_{M1}	EMR %	CMR %
Hybrid action, $a^{-1} = 1.58$ GeV			
$m_\pi = 594(1)$			
0.213	1.850(44)	-0.16(52)	
0.482	1.434(36)	-0.45(67)	-3.52(1.16)
0.738	1.143(41)	-0.52(1.42)	-3.88(1.73)
0.983	0.954(42)		
1.218	0.789(38)		-6.25(2.78)
1.445	0.665(45)		
1.874	0.471(68)		
2.079	0.413(64)		
2.278	0.363(72)		
2.472	0.322(89)		
2.660	0.262(145)		
2.844	0.172(158)		
$m_\pi = 498(3)$			
0.191	1.557(46)	-0.243(91)	
0.471	1.177(38)	-1.14(1.21)	-1.96(1.45)
0.735	0.924(40)	-0.56(2.53)	-0.20(2.42)
0.985	0.783(46)		
1.224	0.641(40)		
1.452	0.565(47)		
1.883	0.371(70)		
2.087	0.381(96)		
2.284	0.294(172)		
2.476	0.260(240)		
2.662	0.104(226)		
2.843	0.146(120)		
$m_\pi = 353(2)$			
0.042(16)	1.681(59)	-0.72(88)	
0.194(14)	1.404(49)	-0.97(1.11)	-2.98(1.06)
0.341(8)	1.199(51)	-0.09(1.824)	-2.41(1.61)
0.482(9)	1.070(48)		
0.619(8)	0.930(47)		-3.82(2.47)
0.751(9)	0.813(48)		
1.005(11)	0.723(53)		
1.127(16)	0.660(53)		
1.246(16)	0.623(60)		
1.362(23)	0.581(62)		
1.475(51)	0.518(89)		
1.586(18)	0.525(84)		
1.695(35)	0.518(94)		
1.906(65)	0.392(116)		
2.009(26)	0.328(87)		
2.111(13)	0.298(94)		
2.209(20)	0.275(128)		
2.306(23)	0.230(94)		
2.402(34)	0.222(124)		
2.497(34)	0.073(108)		
2.682(20)	0.087(170)		

TABLE V: Results in the hybrid approach for \mathcal{G}_{M1} , EMR and CMR. For the smallest quark mass we include the errors in the determination of Q^2 since these are substantial for the small values of Q^2 allowed on this lattice.